Analytic Performance Bounds on SAR-Image Target Recognition using Physics-Based Signatures

Choongyeun Cho[a], Chen-Pang Yeang[a], and Jeffrey H. Shapiro[a,b]

Massachusetts Institute of Technology
[a]Laboratory for Information and Decision Systems
and [b]Research Laboratory of Electronics
Cambridge, MA 02139 USA

ABSTRACT

In recent years, synthetic aperture radars (SARs) have been used to detect man-made targets and to distinguish them from naturally occurring background. This paper continues development of a fundamental, physics-based approach to assessing the performance of SAR-based automatic target recognition (ATR) systems. A major thrust of this effort is to quantify the performance advantages that accrue when the recognition processor exploits the detailed signatures of the target's component reflectors, e.g., their specularity, their polarization properties, etc. Its purpose is to assess target classification performance of a SAR-based ATR, starting from a foundation of rigorous, physics-based signal models developed from the electromagnetic scattering theory. New lower and upper bounds on the probability of correct classification (PCC) are developed for targets composed of a constellation of geometrically-simple reflectors. The performance discrepancy of a conventional full-resolution processor with respect to an optimal whitening-filter processor is discussed.

Keywords: analytic performance bounds, synthetic aperture radar, target recognition, physics-based signatures

1. INTRODUCTION

In recent years, SAR has been rapidly gaining prominence in applications such as remote sensing, surface surveillance, and ATR. A SAR-based ATR system requires a fast and effective discriminator to suppress natural clutter, to detect the presence of a target, and to classify the type of target from its radar return.[1] Such a system relies on the models for different components of the radar return, namely, the returns from different types of man-made targets, natural clutter, and background noise. Our analysis is founded on a rigorous, physics-based theory which relates the radar return from targets and clutter to their respective physical characteristics through an electromagnetic scattering model, taking into account the effects of the transmitter pulse shape, the antenna beam pattern, and free-space wave propagation.[2–4]

Radar return signals from a target and from clutter sources are modeled via an electromagnetic scattering theory, and a conventional and optimum whitening-filter signal processors are considered. In what follows the radar signal models and the SAR processor models are reviewed. With these models, we show how the optimum multi-component target classification is done, based on a maximum aposteriori probability (MAP) rule. Then we focus on a target setting in which each target component can be located anywhere consistent with an orthogonality condition. We will find easily computed lower and upper bounds on the PCC. In a similar fashion, we deal with a case in which the target components are located at uniformly-distributed random positions within given uncertainty areas.

2. SYSTEM MODELS

2.1. Radar Signal Model

Yeang[3,4] used a first-principles approach to set up signal models of SAR imagery via an electromagnetic scattering theory. We are interested in quantifying, from a fundamental-principles viewpoint, the target-classification performance advantage of the whitening-filter processors compared with that of the conventional SAR imagers. Thus the multi-component target models we shall employ will not be as complicated as real-world objects. Instead they

Send correspondence to J. H. Shapiro, Email: jhs@mit.edu; Phone: 617-253-4179; FAX: 617-253-1301
Research supported by U.S. Air Force Office of Scientific Research Grant F49620-96-1-0028

Algorithms for Synthetic Aperture Radar Imagery VIII, Edmund G. Zelnio, Editor,
Proceedings of SPIE Vol. 4382 (2001) © 2001 SPIE · 0277-786X/01/$15.00

will be simple reflector constellations that embody the characteristics which will highlight the performance differences between the conventional SAR full-resolution processing and the optimum whitening-filter-based processing. In particular, the targets will consist of specular mirrors (square flat plates with perfectly conducting surfaces), and dihedrals (pairs of perfectly-conducting rectangular plates whose edges meet at right angles). The PCC bounds that we develop can, for the most part, be extended to treat other reflectors, such as trihedrals and dielectric volumes. In addition to the target return, the clutter needs to be modeled. Clutter typically refers to the radar return from anything other than the desired target. We will assume the clutter to be a reflection from an infinitely extended rough ground surface. The final element in the radar signal model is the receiver noise. Typically, this is a thermal noise, and has a white spectrum. The receiver noise is assumed to be a zero-mean, circulo-complex, vector-Gaussian stochastic process that is white in all domains. We deal with stripmap-mode operation throughout the paper; the change of modes does not affect our analysis of classification performance.

2.2. SAR Processor Models

Conventional processor:

Figure 1 illustrates a conventional full-resolution processor for stripmap-mode operation; the incoming radar return is passed through chirp compression filters in both the cross-range and the range domains, and then is detected to form a radar intensity image. The sampling times, m and τ, correspond to the center location of a target reflector in a cross-range-time and range-time domain, respectively. An adaptive-resolution processor can be built upon this conventional SAR architecture by using adjustable processing durations in the chirp compression filters.

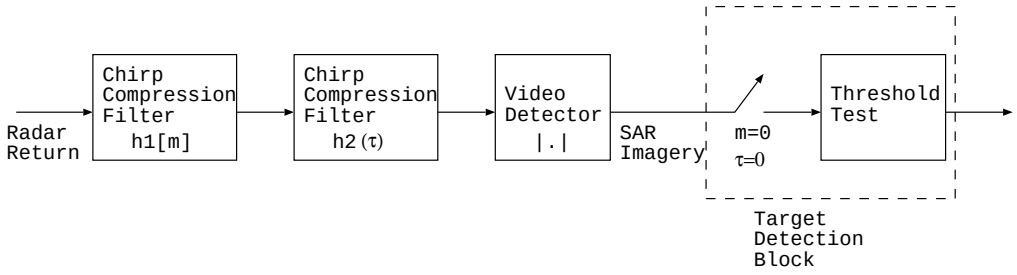

Figure 1. Block diagram of conventional stripmap-mode SAR processor for detecting a single reflector at a known location

Whitening processor:

The optimum Neyman-Pearson processing scheme for detecting a single reflector at a known location uses a filter to whiten the clutter-plus-noise, followed by a matched filter corresponding to the target-return waveform passed through the whitening filter, followed in turn by the video detection, sampling, and a threshold test. The whitening-

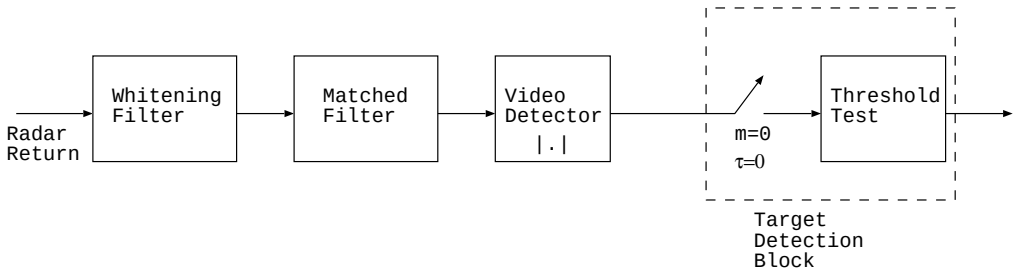

Figure 2. The whitening-filter optimum processor for detecting a single reflector at a known location

filter processor, shown in Figure 2, is seldom as practical as the conventional processor because it requires exact

knowledge of the clutter and the noise statistics, and the waveforms scattered from the target types of interest. Nevertheless, the whitening-filter processor is conceptually important because it is the optimum processor for target classification. As such, its performance in terms of probability of correct classification bounds the performance of any realizable processor. By comparing the classification performance of a conventional processor with that of a whitening processor, we can determine how far the conventional processor's classification performance is from the ultimate theoretical limit.

2.3. Multi-component Target Classification

A multi-component target is a collection of simple reflectors located at different positions. The radar-return signal from a multi-component target is the sum of the contributions from all the individual scatterers. Multiple scattering between different reflectors is neglected. A multi-component target classification problem is formulated in the following manner. Let $\mathbf{r}(m,\tau)$ be the radar return from a multi-component target after passing through a whitening filter. Therefore, it has the unwanted clutter-plus-noise component whitened to unity spectral density. We use the boldface symbol to denote the fully polarimetric return signal (HH, VV, and HV where the vertical polarization aligns with the aircraft flight direction). Then, if H_i denotes that target i among all N possible targets is present, $\mathbf{r}(m,\tau)$ can be written as follows:

$$\text{under } H_i: \qquad \mathbf{r}(m,\tau) = \sum_{p=1}^{M_i} e^{i\phi_{p^i}} \mathbf{s}_{p^i}(m - m_{p^i}, \tau - \tau_{p^i}) + \mathbf{w}(m,\tau) \text{ for } i = 1, ..., N. \tag{1}$$

Here $\mathbf{w}(m,\tau)$ is the vector clutter-plus-noise complex envelope after the whitening filter. By construction it is white in the cross-range-time (m), the range-time (τ) and the polarimetric (vector) domains. Likewise, $\mathbf{s}_{p^i}(m,\tau)$ corresponds to the post-whitening-filter radar-return complex envelope from the p-th component of the i-th target when the component is located at the scene center. The time delays m_{p^i}, τ_{p^i} for this component are determined by its actual location. The phases $\{\phi_{p^i}\}$ are independent random variables that are uniformly distributed within $[0, 2\pi)$; they represent the incoherence of each target-component with respect to other components as well as the noise. When the spatial separations between the individual target components are large enough, the following orthogonality condition prevails:

$$\sum_{m=-\infty}^{\infty} \int_{-\infty}^{\infty} d\tau \ \mathbf{s}_i^{\dagger}(m - m_i, \tau - \tau_i) \cdot \mathbf{s}_j(m - m_j, \tau - \tau_j) \approx 0 \tag{2}$$

for any two components located at different positions.

We can develop a target classifier for a repertoire of multi-component targets based on the single-target detectors. Based on a MAP rule, a single-target detector can be constructed by passing the radar-return signal through a bank of matched filters (matched to all target reflectors) and then combining the outputs from the matched filters. Specifically, the likelihood ratio for MAP target detection is

$$l_1(\mathbf{r}) = \frac{p_{\mathbf{r}|H_1}(r_1, r_2, ..., r_M|H_1)}{p_{\mathbf{r}|H_0}(r_1, r_2, ..., r_M|H_0)} = \prod_{m=1}^{M} \exp[-E_m] I_0(2|r_m|) \tag{3}$$

where hypothesis H_0 means the target is absent, H_1 means the target is present, E_m is the energy of the m-th component return, and I_0 is the zeroth-order modified Bessel function. Here, $\mathbf{r}$ is the vector of the matched-filter outputs sampled at the proper times; it has the complete information about the whole radar return signal needed for the classification operation. At the target detector's output stage, a value equal or proportional to the likelihood ratio is compared with a threshold level in order to decide on the absence or presence of that target. When there is more than one possible target type, we can pass the radar return through a bank of target detectors, one for each target type. The resulting real-valued output levels l_1, ..., l_N are the likelihood ratios of conditions H_1, ..., H_N with respect to condition H_0 (clutter and noise only). To carry out classification, we select their maximum value; if l_p is maximum among l_1, ..., l_N, then the classifier decides the target to be type p.

A conventional SAR target classifier can also be constructed by combining the corresponding conventional SAR target detectors in the similar manner.

3. TARGET WITH KNOWN REFLECTOR POSITIONS

3.1. Classification Scheme

Evaluation of the performance of multi-component target classification is computationally intensive, because the likelihood values of different multi-component targets are densely correlated in general. Within the scope of this paper, we assume that each target component can be located anywhere provided the orthogonality condition (2) holds. For the upper bound and the lower bound on the PCC developed in this section, the target components are assumed to be fixed at known positions, and the phase of the target signal from each component is randomly distributed in a uniform fashion, which represents the unavailability of accurate relative phase information between the various components of a multi-reflector target. The radar return model under this target condition is specified by (1) and the time delays corresponding to the target component locations (m_{p^k}, τ_{p^k}) are presumed known. The

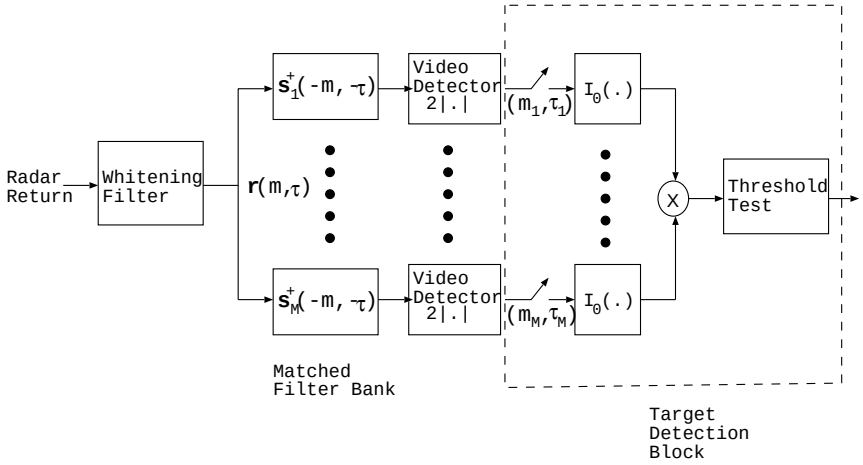

Figure 3. Block diagram of likelihood-ratio detector for a target with unknown reflector phases

block diagram of the likelihood-ratio target detector is shown in Figure 3. To build a target classifier we employ a bank of likelihood-ratio (LR) detectors with one slight modification. After each Bessel-function operation in a target detector, we need to normalize the output value by $\exp(-E_{p^i})$ where E_{p^i} is the output energy of target i's component p^i. The normalized output is a likelihood ratio, l_i, of condition H_i with respect to condition H_0. To carry out classification, we do not pass the $\{l_k\}$ through individual threshold comparators, but select the maximum.

3.2. Lower Bound on the PCC

A lower bound on the PCC can be calculated by finding PCC for any sub-optimal classifier. For a sub-optimal classifier, we will use a component-wise detection rule. Suppose that the components are mutually orthogonal and that only two reflector types — specular and dihedral — are considered. Then, we can discriminate the reflector type for each component separately, and use these component decisions as inputs to a (sub-optimum) MAP M-ary decision rule. We can regard the decision for each target component as establishing a binary discrete memoryless channel (DMC), with transition probabilities calculated from the model in Figure 4. For a general target setting, a ternary DMC is employed to incorporate an additional "null" reflector. The detection scheme for three target reflectors including a "null" reflector is similar to that shown in Figure 4 except we have one additional value, 1 to be compared with the two other outputs from matched filters, i.e., those matched to the dihedral and specular reflectors. Combining the transition probabilities of the DMC with an M-ary decision rule based on the DMC then yields an easily calculated error probability from which a PCC lower bound immediately follows. This method of obtaining a lower bound on the PCC can also be applied to the conventional full-resolution imager.

3.3. Upper Bound on the PCC

Obtaining an upper bound on the PCC is equivalent to finding a lower bound on the error probability. If the reflector phases were exactly known and optimally employed, then the error probability would not be higher than the case

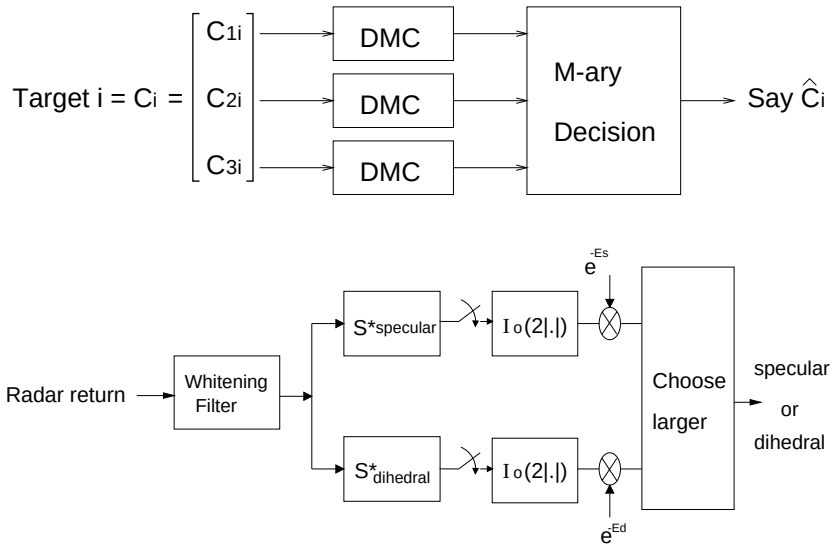

Figure 4. Upper panel represents a target classifier for three-component targets based on component-wise detection. Lower panel shows a model for a discrete memoryless channel.

in which the phases of all components are random. Given exact phases, the classification problem simply becomes an M-ary detection of the signals in an additive white Gaussian-noise channel. In general, the error probability of detection of M signals over the additive white-Gaussian noise channel is not available in a closed form. Thus, we again use a lower bound on this error probability.

$$\begin{aligned} \text{PCC} &= \sum_{i=1}^{N} \Pr(\textit{say } H_i \mid H_i \textit{ true}) \Pr(H_i) && (4) \\ &= \sum_{i=1}^{N} \{1 - \Pr(\textit{error} \mid H_i \textit{ true})\} \Pr(H_i). && (5) \end{aligned}$$

$$\begin{aligned} \Pr(\textit{error} \mid H_i \textit{ true}) &\geq \Pr(\textit{error} \mid H_i \textit{ true, phase information given}) && (6) \\ &= \Pr(\bigcup_{j \neq i} \mathcal{E}_{ij} \mid H_i \textit{ true, phase information given}). && (7) \end{aligned}$$

Here $\mathcal{E}_{ij}$ denotes the case $\{\|\mathbf{s}' - \mathbf{s}_j\| \leq \|\mathbf{s}' - \mathbf{s}_i\|\}$ where $\mathbf{s}'$ is a matched-filter-output vector, matched to all distinct target-components, and properly normalized to make the noise part circulo-complex Gaussian with unit-variance. $\mathbf{s}_i$ is the mean of $\mathbf{s}'$ when the target i is present. The prior probability of target i, $\Pr(H_i)$, will be assumed to be $1/N$, i.e., all targets will be assumed equiprobable.

De Caen's inequality[5] can be used to get a lower bound on the probability of a union:

$$\Pr(\bigcup_{j=1}^{N} A_j) \;\geq\; \sum_j \frac{\Pr(A_j)^2}{\sum_k \Pr(A_j \cap A_k)}. \tag{8}$$

Applying this inequality to the probability of error, we obtain

$$\Pr(\textit{error} \mid H_i \textit{ true, phase information given}) \;\geq\; \sum_{j \neq i} \frac{Q^2(d_{ij}/2)}{\sum_{k \neq i} \Psi(\rho_{jk}, d_{ij}/2, d_{ik}/2)} \tag{9}$$

where

$$d_{ij} = \|\mathbf{s}_i - \mathbf{s}_j\|, \;\; \rho_{jk} = \frac{< \mathbf{s}_i - \mathbf{s}_j, \mathbf{s}_i - \mathbf{s}_k >}{\|\mathbf{s}_i - \mathbf{s}_j\| \|\mathbf{s}_i - \mathbf{s}_k\|}, \;\; Q(x) = \frac{1}{\sqrt{2\pi}} \int_x^\infty \exp(-y^2/2) dy,$$

Flight Parameters	Radar Parameters	Reflector Parameters
aircraft altitude $L = 5000\,\mathrm{m}$	antenna radii $a_x = a_y = 1\,\mathrm{m}$	target radii $\rho_t = 1.5\,\mathrm{m}$
aircraft speed $v = 100\,\mathrm{m/s}$	Tx and LO powers $P_T = P_{LO} = 1\,\mathrm{W}$	relative permittivity $\epsilon_r = 10 + i5$
slant angle $\psi = 45°$	radar frequency $f_c = \Omega_c/2\pi = 10\,\mathrm{GHz}$	HV clutter strength $\epsilon = 0.2$
	pulse-repetition period $T_s = 10\,\mathrm{ms}$	HH×VV correlation $\rho = 0.57$
	pulse width $T_0 = 0.05\,\mu\mathrm{s}$	
	chirp bandwidth $W_0 = 100\,\mathrm{MHz}$	

Table 1. Parameter values for signal-to-noise-plus-clutter calculations

	Target 1	Target 2	Target 3
Component 1 type / center location	specular / (0 m, 0 m)	specular / (0 m, 0 m)	specular / (0 m, 0 m)
Component 2 type / center location	specular / (-7 m, -3 m)	specular / (-7 m, -3 m)	dihedral / (-7 m, -3 m)
Component 3 type / center location	specular / (5 m, -5 m)	dihedral / (5 m, -5 m)	dihedral / (5 m, -5 m)

Table 2. Specification of target constellation for the example. Note that the orientation angle of all specular reflectors (the angle between the slant range and the normal direction of the plate) is 0°, and the orientation angle of all dihedral reflectors (the angle between the SAR flight path direction and the dihedral axis) is 45°. The side lengths of all target components are 0.5 m.

$$\Psi(\rho_{jk}, d_{ij}/2, d_{ik}/2) \;=\; \frac{1}{2\pi\sqrt{1-\rho_{jk}^2}} \int_{d_{ij}/2}^{\infty} \int_{d_{ik}/2}^{\infty} \exp(-\frac{x^2 - 2\rho_{jk}xy + y^2}{2(1-\rho_{jk}^2)}) dx\, dy.$$

This inequality deals with only two joint Gaussian random variables, and we have all the constants needed for its evaluation, namely, the distances between all signal points. The error probability bound is thus easy to calculate. Like the lower bound on the PCC, this upper bound can be applied to all processor models and both SAR operation modes.

For the following examples, we will use the radar geometries and the radar parameters specified in Table 1. These values are not far from the specification of a real system.[6] Figure 5 compares the bounds on the PCC of the conventional classifier to the PCC of the optimal whitening-filter classifier for the 3-component target constellation specified in Table 2. PCC values are plotted with respect to the clutter-to-noise ratio (CNR). The quantity 1/CNR measures the intensity of the noise with respect to a fixed clutter level. As the noise level increases, the two lower bounds converge asymptotically to 1/3, which is the appropriate result: when the noise intensity is very high, the classification operation simply becomes a blind guess. The PCC results from a 5000-trial computer simulation are also plotted. The simulation results turn out to be very close to the lower bound. We can see that the optimal classifier has a gain of about 6 dB in the value of the signal-to-noise-plus-clutter ratio (SNCR). There are three factors that lead to the whitening-filter processor's performance advantage over the conventional SAR processor's performance: the effect of the whitening filter, the polarimetric effect, and the adaptive-resolution effect. Because the conventional processor makes use of only a single polarization (HH) whereas the whitening-filter processor takes full advantage of all polarimetric components, the whitening-filter processor has a 3 dB enhancement of its SNCR value. The additional (approximately) 3 dB gain of the whitening-filter processor comes from the adaptive-resolution effect and the whitening of clutter plus noise.

To highlight the difference between the PCC lower bound developed in this paper and the one in previous work by Yeang,[3] we first compare his PCC lower bound for the example shown in Figure 5,

$$\mathrm{PCC} \;\geq\; \frac{1}{3}(Q_1^2 + Q_1Q_2 + Q_2^2), \tag{10}$$

to our PCC lower bound

$$\mathrm{PCC} \;\geq\; \frac{1}{3}\{\max(Q_1^2, Q_2^2) + Q_1Q_2 + \min(Q_1, Q_2)\}. \tag{11}$$

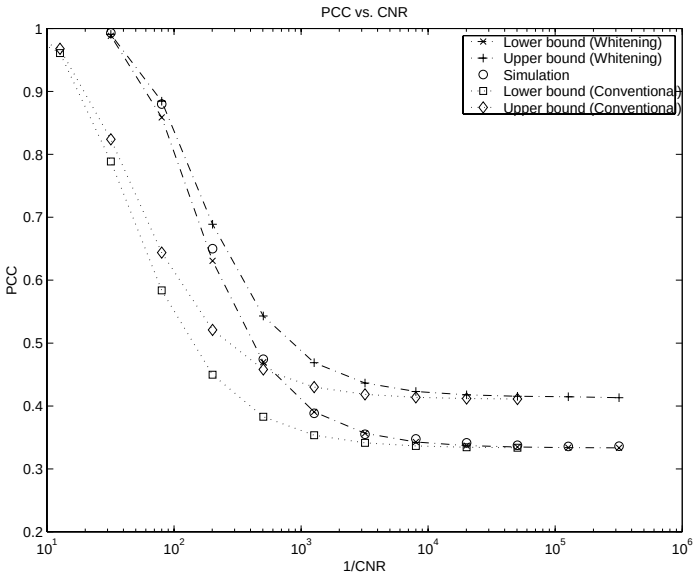

Figure 5. PCC for whitening filter processor and conventional processor

Here, $Q_1 \equiv \Pr(\textit{say specular} \mid \textit{specular is true})$, and $Q_2 \equiv \Pr(\textit{say dihedral} \mid \textit{dihedral is true})$ are the transition probabilities of the DMC. It is easy to see that the PCC lower bound developed in this paper (11) is always tighter than Yeang's lower bound (10). Figure 6 plots these PCC lower bounds, Yeang's upper bound, our upper bound, and the results from a 5000-trial computer simulation. We observe a few features in Figure 6. First, the new lower bound derived in this paper converges to the true PCC value of 1/3 as CNR goes to 0, whereas Yeang's lower bound is substantially lower in the high-noise regime. Second, Yeang's upper bound is tighter than the upper bound obtained in 3.3. We must note, however, that Yeang's upper and lower bounds rely on the special symmetries of the target reflector constellation presented in this example, whereas our bounds can be applied to any target setting which obeys the orthogonality condition. In the following example, we will obtain the lower bound and the upper bound on the PCC of a whitening-filter-based classifier for a target component setting which cannot be handled by the previous approach.

3.4. Example

In this 4-target example, each target consists of 10 reflectors with different locations, orientations, sizes and types as specified in Table 3. The upper and lower bounds on the PCC previously developed are calculated for this target constellation. Figure 7 plots the PCC bounds versus the inverse of the CNR for both the conventional classifier and the optimal whitening-filter processor when both have perfect knowledge of target location. Also included in this figure are PCC results obtained from 50000-trial computer simulations of these two processors. Figure 7 shows that the PCC lower bound for the whitening-filter processor is close to its simulation result. For the conventional processor, the simulation shows that the PCC approaches a sub-unity, clutter-limited value in the limit of zero noise, i.e., when $1/\text{CNR} \to 0$. Figure 7 also shows that the whitening-filter classifier has about 5 dB gain in terms of the SNCR as compared with the conventional processor. This advantage is due to the combined benefits accruing from whitening-filter processing (which optimally suppresses clutter), full polarimetric processing (which only the optimal processor was presumed to have), and adaptive-resolution processing (which the optimal system uses to exploit physics-based signatures of the various reflector components).

4. TARGET WITH UNCERTAIN REFLECTOR POSITIONS

4.1. Classification Scheme

In this section, we explore the classification of the targets with uncertain reflector positions. Incorporating the position uncertainty of the reflector components, the radar return for each hypothesis is modeled in the same form

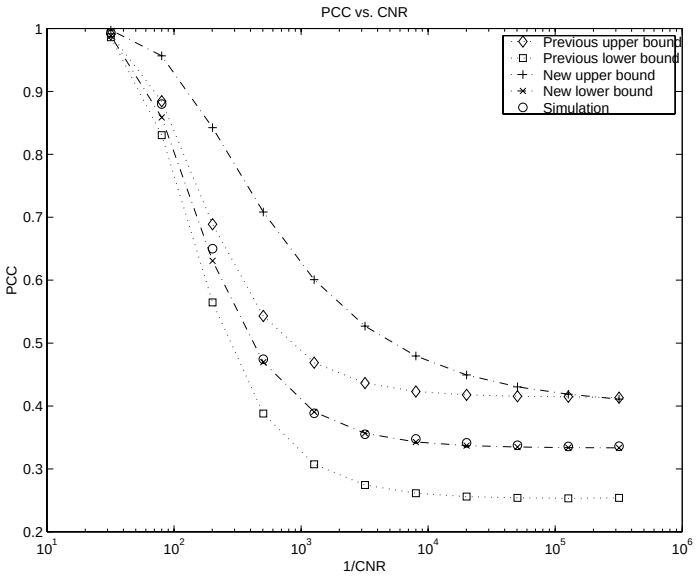

Figure 6. Yeang's PCC bounds and new bounds

Target 1				Target 2				Target 3				Target 4			
x, y	θ, ϕ	ρ	t	x, y	θ, ϕ	ρ	t	x,y	θ, ϕ	ρ	t	x,y	θ, ϕ	ρ	t
2.5 -0.2	-90 45	5	S	-2.7 -0.7	-88 46	4	S	2.5 -0.2	-90 45	5	S	-2.7 -0.7	-88 46	4	S
0.6 -0.5	-91 45	4	S	0.6 -0.5	-91 45	4	S	0.3 1.4	-90 43	10	D	0.6 -0.5	-91 45	4	S
-2.0 -1.5	-90 45	9	S	-0.2 -0.5	-88 47	16	D	-0.2 -0.5	-88 47	16	D	-0.2 -0.5	-88 47	16	D
-1.0 0.6	-90 44	15	S	-0.6 -1.0	-93 43	6	D	2.0 1.0	-90 45	16	S	2.0 1.0	-90 45	16	S
-2.5 -0.8	-90 43	5	D	-2.5 -0.8	-90 43	5	D	-1.2 1.3	-88 44	10	S	-2.5 -0.8	-90 43	5	D
1.2 -1.6	-93 44	8	S	1.2 -1.6	-93 44	8	S	-1.5 1.0	-90 45	13	D	1.2 -1.6	-93 44	8	S
3.0 -1.5	-90 45	16	S	-0.7 -0.1	-85 43	19	D	-0.7 -0.1	-85 43	19	D	3.0 -1.5	-90 45	16	S
0.6 -0.7	-93 43	6	D	2.7 -1.0	-89 46	13	S	2.7 -1.0	-89 46	13	S	0.6 -0.7	-93 43	6	D
1.5 -1.0	-92 45	8	S	0.2 -1.5	-90 49	9	D	1.5 -1.0	-92 45	8	S	0.2 -1.5	-90 49	9	D
-0.6 1.4	-90 44	15	S	1.2 -1.3	-85 45	5	D	-1.3 -1.0	-87 42	18	D	-1.3 -1.0	-87 42	18	D

Table 3. Specification of target constellation for the example. Note that (x, y) is the center location (in m), θ, ϕ are polar and azimuthal angles ($^\circ$), and ρ is half the side length of a reflector (in cm). "S" and "D" in columns denoted by "t" stand for specular and dihedral reflector, respectively.

as that in (1) except the center locations $(m_{p^k},\, \tau_{p^k})$ of the target components are no longer fixed and known. The random variables m_{p^k}, τ_{p^k} are assumed to be mutually independent and each random variable is uniformly distributed within $[m^0_{p^k} - M_{p^k}/2, m^0_{p^k} + M_{p^k}/2]$ for m_{p^k} and $[\tau^0_{p^k} - T_{p^k}/2, \tau^0_{p^k} + T_{p^k}/2]$ for τ_{p^k}. The position randomness models the variability or unavailability of the exact knowledge about some aspects of a target reflector constellation in the real world.

Because the delay times are uniform random variables, it is difficult to write down the likelihood ratio of two different hypotheses. We can, however, formulate the generalized likelihood ratio and develop a target classifier on that basis. For a specific realization of the delay times, the likelihood ratio of hypotheses H_k (target k) with respect to the null hypotheses H_0 (clutter plus noise only) is:

$$l_k(\mathbf{r}; m_1, ..., m_{M_k}, \tau_1, ..., \tau_{M_k}) \quad = \quad \frac{p_{\mathbf{r}|H_k}(r_1, r_2, ..., r_{M_k}|H_k; m_1, ..., m_{p^k}, \tau_1, ..., \tau_{M_k})}{p_{\mathbf{r}|H_0}(r_1, r_2, ..., r_{M_k}|H_0; m_1, ..., m_{p^k}, \tau_1, ..., \tau_{M_k})}$$

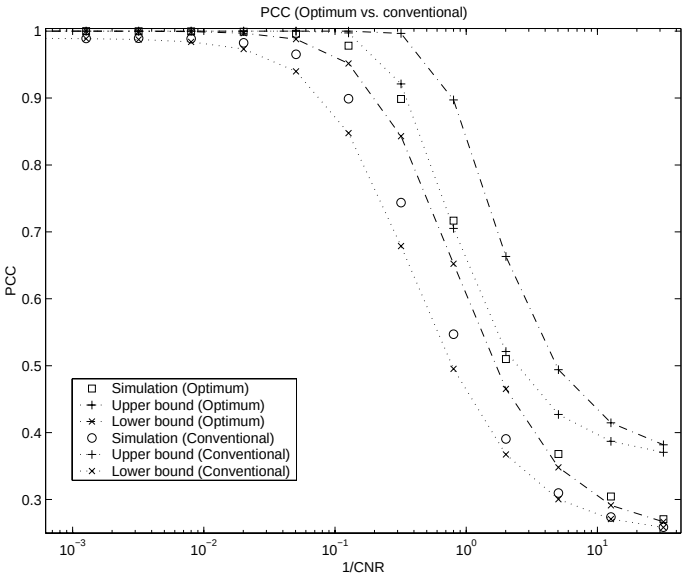

Figure 7. PCC upper and lower bounds for the target constellation specified in Table 3

$$= \prod_{p=1}^{M_k} \exp(-E_{p^k}) I_0 \left(2 \left| \sum_m \int_{-\infty}^{\infty} d\tau \mathbf{s}_{p^k}^{\dagger}(m - m_{p^k}, \tau - \tau_{p^k}) \cdot \mathbf{r}(m,\tau) \right| \right), \quad (12)$$

where E_{p^k} is the energy of p-th component of k-th target. For a given radar return $\mathbf{r}(m,\tau)$, the likelihood ratio is a function of m_1,...,m_{M_k},τ_1,...,τ_{M_k}. The maximum-likelihood estimate of these parameters from the radar return is:

$$\left[\ \hat{m}_1 ... \hat{m}_{M_k} \ \hat{\tau}_1 ... \hat{\tau}_{M_k} \ \right] = \arg \ \max \prod_{p=1}^{M_k} \exp(-E_{p^k}) I_0 \left(2 \left| \sum_m \int_{-\infty}^{\infty} d\tau \mathbf{s}_{p^k}^{\dagger}(m - m_{p^k}, \tau - \tau_{p^k}) \cdot \mathbf{r}(m,\tau) \right| \right) \quad (13)$$

where $\hat{m}_1$, ..., $\hat{m}_{M_k}$, $\hat{\tau}_1$, ..., $\hat{\tau}_{M_k}$ are the maximum-likelihood estimates over $m_1 \in [m_1^0 - M_1/2, m_1^0 + M_1/2], ..., m_{M_k} \in [m_{M_k}^0 - M_{M_k}/2, m_{M_k}^0 + M_{M_k}/2]$ and $\tau_1 \in [\tau_1^0 - T_1/2, \tau_1^0 + T_1/2], ..., \tau_{M_k} \in [\tau_{M_k}^0 - T_{M_k}/2, \tau_{M_k}^0 + T_{M_k}/2]$. The generalized likelihood ratio is defined as the likelihood ratio when the unknown parameters are replaced by their maximum-likelihood estimates. Plugging (13) into (12), we have that:

$$\begin{aligned} \text{GLR} &= l_k(\mathbf{r}; \hat{m}_1, ..., \hat{m}_{M_k}, \hat{\tau}_1, ..., \hat{\tau}_{M_k}) \\ &= \max \prod_{p=1}^{M_k} \exp(-E_{p^k}) I_0 \left(2 \left| \sum_m \int_{-\infty}^{\infty} d\tau \mathbf{s}_{p^k}^{\dagger}(m - m_{p^k}, \tau - \tau_{p^k}) \cdot \mathbf{r}(m,\tau) \right| \right). \end{aligned} \quad (14)$$

The generalized-likelihood-ratio detector based on (14) can be written in the following form:

$$\max \prod_{p=1}^{M_k} \left[I_0 \left(2 \left| \sum_m \int_{-\infty}^{\infty} d\tau \mathbf{s}_{p^k}^{\dagger}(m - m_{p^k}, \tau - \tau_{p^k}) \cdot \mathbf{r}(m,\tau) \right| \right) \right] \begin{array}{c} \text{say } H_k \\ > \\ < \\ \text{say } H_0 \end{array} \beta \quad (15)$$

where β is the threshold and the maximum is over the same domain as that in (14). Furthermore, because the zeroth-order modified Bessel function is monotonically increasing and m_1, ..., m_{M_k}, τ_1, ..., τ_{M_k} are mutually independent variables, maximizing the overall product of I_0's in (15) is equivalent to maximizing the individual I_0's in the product.

Hence the generalized-likelihood-ratio detector becomes

$$\prod_{p=1}^{M_k} \max \left[I_0 \left(2 \left| \sum_m \int_{-\infty}^{\infty} d\tau \mathbf{s}^{\dagger}_{p^k}(m - m_{p^k}, \tau - \tau_{p^k}) \cdot \mathbf{r}(m, \tau) \right| \right) \right] \begin{array}{c} \text{say } H_k \\ > \\ < \\ \text{say } H_0 \end{array} \beta. \tag{16}$$

The form of the GLR detector is similar to the LR detector discussed in the previous section except that in the GLR detector the value used to compare the threshold is maximized over the region of the delay-time uncertainty. This operation can be achieved by inserting a duration-limited peak detector after the video detection of the output from each individual matched filter. Figure 8 sketches the block diagram of the generalized-likelihood-ratio detector. A target classifier can be built, as discussed in the previous section, by employing a bank of target detectors, incorporating energy corrections, and choosing the largest output level.

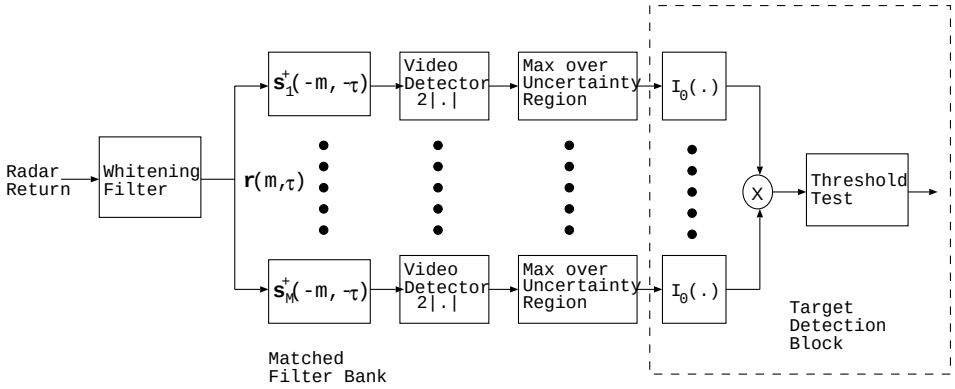

Figure 8. Block diagram of generalized-likelihood-ratio detector for a target with unknown reflector phases and uncertain reflector positions

In order to calculate the PCC for the M-ary target recognition problem, we need to obtain the statistical structure of the generalized likelihood ratio. As implied by (16), in order to obtain the statistics of the GLR we must solve the following general level-crossing problem: for a complex 2-D random process with a given covariance function and a fixed real-valued threshold level, what is the probability that the magnitude of this random process is smaller than the threshold level within a given area. When the target is absent or all the components are mismatched to the detector's filters, then this random process is approximately stationary. When at least one of the target components is matched to the detector's filters, this process is non-stationary. As a result it is best to consider the level-crossing problems for H_0 and H_k ($k \neq 0$) separately.

4.2. Lower bound on the PCC

Paralleling the work in the last section, a component-wise detector can be exploited to obtain a lower bound on the PCC for the random-position case. Any sub-optimal classifier will be inferior in its classification performance to the optimum one. Thus, the PCC for a sub-optimal target recognizer is a valid PCC lower bound for an optimum classifier. Figure 9 depicts the block diagram of a component-wise detector. This detector can be seen to be the optimum target classifier for two single-reflector (specular or dihedral) targets. We carry out a binary detection for each reflector component, and then collect the results from each component-wise detector to make a MAP M-ary decision. This is a valid classification scheme, but not necessarily the optimum one. For our general target setting, the component-wise detector incorporates a null reflector by choosing the largest output among l_s (specular), l_d (dihedral) and 1 (no reflector). To obtain the PCC for this sub-optimal classifier, we only need to know the transition probabilities for the component-wise detector. Assume the true target component is specular. We have that the transition probability, $Q_1 \equiv \Pr(\textit{say specular} \mid \textit{specular is true})$, satisfies

$$Q_1 \quad = \quad \Pr(l_s > l_d \mid \textit{specular is true}) \tag{17}$$

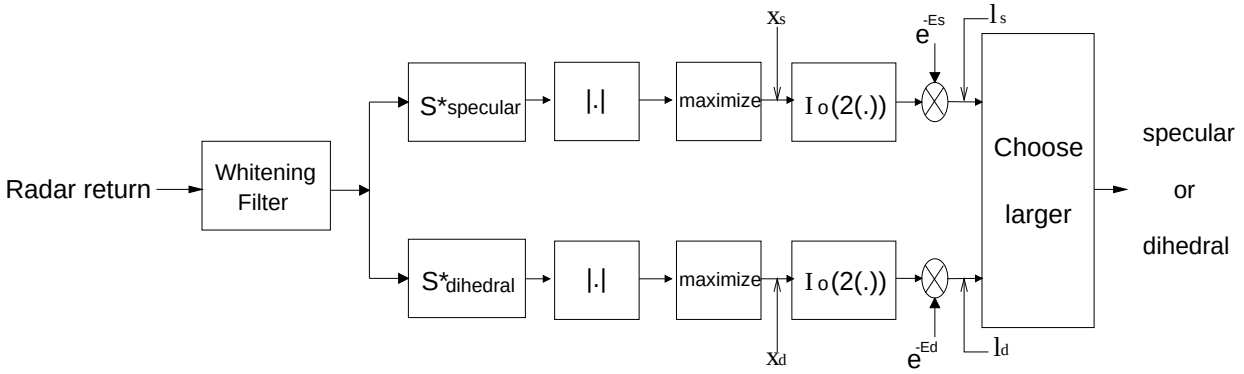

Figure 9. Block diagram of component-wise detector

$$= \Pr\left(I_0(2x_s)e^{-E_s} > I_0(2x_d)e^{-E_d} \mid \textit{specular is true}\right) \tag{18}$$

$$= \Pr\left(x_s > \frac{1}{2}I_0^{-1}(e^{E_s-E_d}I_0(2x_d)) \mid \textit{specular is true}\right) \tag{19}$$

$$= 1 - \Pr\left(x_s < \frac{1}{2}I_0^{-1}(e^{E_s-E_d}I_0(2x_d)) \mid \textit{specular is true}\right) \tag{20}$$

$$= 1 - \int_0^\infty dX_d\, p_{x_d|specular}(X_d \mid \textit{specular is true}) \Pr(x_s < \gamma \mid \textit{specular is true}) \tag{21}$$

where $\gamma = \frac{1}{2}I_0^{-1}(e^{E_s-E_d}I_0(2X_d))$.

To evaluate the last term, we need to know the probability structure of x_s and x_d. We treat $p(x_s \mid \textit{specular is true})$ and $p(x_d \mid \textit{specular is true})$ separately, because their statistical behaviors are quite different. For x_s, the radar return is passed through a filter which is matched to that of the specular return signal. The maximization process will pick up the peak value of the magnitude of the post-matched-filter signal within the uncertainty region. If we partition the uncertainty region into resolution bins and assume that each bin is statistically independent of the others, we can formulate the cumulative distribution function (CDF) of x_s as follows:

$$\Pr(x_s < \gamma \mid \textit{specular is true}) = \mathrm{P}_1{}^{N-1}(\gamma)\mathrm{P}_2(\gamma) \tag{22}$$

where N is the number of bins, $\mathrm{P}_1(\gamma)$ is the probability that the magnitude of the stationary whitened clutter-plus-noise is always less than γ for a given bin area, and $\mathrm{P}_2(\gamma)$ is the CDF of the output value from a perfectly matched signal sampled at the correct position. $\mathrm{P}_1(\gamma)$ can be calculated by applying 2-D level-crossing theory, and $\mathrm{P}_2(\gamma)$ can be obtained analytically.

For the x_d case, the radar return from a specular reflector is matched to the dihedral signal. Thus, x_d will be stationary over the whole uncertainty region. We can, again, apply the 2-D level crossing theory to obtain the CDF of x_d. Since we know the statistics of x_s and x_d, we can now evaluate the transition probability Q_1:

$$Q_1 = 1 - \int_0^\infty dX_d\, p_{x_d|specular}(X_d \mid \textit{specular is true})\mathrm{P}_1{}^{N-1}(\gamma)\mathrm{P}_2(\gamma). \tag{23}$$

We can find $Q_2 \equiv \Pr(\textit{say dihedral} \mid \textit{dihedral is true})$ in a similar way. Having both transition probabilities, Q_1 and Q_2, we can make an M-ary decision based on the MAP rule and obtain our component-wise lower bound on the PCC for the case of position uncertainty.

4.3. Upper bound on the PCC

To get an upper bound on the PCC we assume that we have exact phase information for each reflector. Because this means we have more information for the classification task, the PCC for the optimum receiver in this case will be a valid upper bound on the PCC in the case of target with random phases, which we are interested in. If we assume

all target components are orthogonal, we can set the phases to be zero for all target component signals without loss of generality. Thus the formula for the radar return signal is similar to (1) except that all $e^{i\phi_p}$ terms are left out. Using this return signal model, the likelihood ratio for the target k with respect to target 0 (the null hypothesis) is:

$$l_k(\mathbf{r}; m_1, ..., m_{M_k}, \tau_1, ..., \tau_{M_k}) = \prod_{p=1}^{M_k} \exp\left(-E_{p^k} + 2\Re\{\sum_m \int_{-\infty}^{\infty} d\tau \mathbf{s}_{p^k}^{\dagger}(m - m_{p^k}, \tau - \tau_{p^k}) \cdot \mathbf{r}(m, \tau)\} \right) \tag{24}$$

where E_{p^k} is the energy of p-th component of k-th target. It is similar to (12) but does not involve a Bessel function. The generalized log likelihood ratio (GLLR) for the target k is thus:

$$\begin{aligned} \mathrm{GLLR}_k &= \sum_{p=1}^{M_k} \left(-E_{p^k} + 2 \max \Re\{\sum_m \int_{-\infty}^{\infty} d\tau \mathbf{s}_{p^k}^{\dagger}(m - m_{p^k}, \tau - \tau_{p^k}) \cdot \mathbf{r}(m, \tau)\} \right) & (25) \\ &= \sum_{p=1}^{M_k} \left(-E_{p^k} + 2y_{p^k} \right). & (26) \end{aligned}$$

Here, the statistics of y_{p^k} can be calculated via level crossing theory. The probability of correct classification can then be evaluated via

$$\begin{aligned} \mathrm{PCC}|H_i &= 1 - \Pr(\textit{error} \mid H_i \textit{ is true}) & (27) \\ &\leq 1 - \Pr(\textit{error} \mid H_i \textit{ is true}, \textit{phase information given}) & (28) \\ &= 1 - \Pr(\bigcup_{\forall j \neq i} \{\mathrm{GLLR}_i < \mathrm{GLLR}_j\} \mid H_i \textit{ is true}, \textit{phase info given}) & (29) \\ &\leq 1 - \max_{j \neq i} \Pr(\mathrm{GLLR}_i < \mathrm{GLLR}_j \mid H_i \textit{ is true}, \textit{phase info given}). & (30) \end{aligned}$$

In the previous section we used de Caen's inequality (8) to obtain a tighter lower bound on the probability of a union, which involves the joint probability distribution of two Gaussian random variables. However, for this target setting, we cannot apply de Caen's inequality in (29) because the statistics of GLLR_i are complicated. The formula (30) can be calculated without difficulty since we have the statistics for the GLLR's.

4.4. Example

We obtained the lower and upper bounds on the PCC for the target setting specified in Table 3, but with uncertain locations. The uncertain areas for the target reflectors were all set to squares with side length of 30 cm. The left panel in Figure 10 compares the lower and upper bounds on the PCC for the optimum whitening classifier with those for the conventional classifier. Also included in this figure are the PCC results for these processors obtained via 50000-trial computer simulations. Figure 10 presents similar features to those seen earlier for the known-reflector-position example. Thus, although the PCC lower bound for the whitening processor is somewhat looser when compared with the simulation result, the optimal classifier still has about 5 dB SNCR gain relative to the conventional classifier. Note that there is a considerable gap, for the conventional processor, between the PCC lower bound and the simulation result, and neither of these curves approaches unity as $1/\mathrm{CNR} \to 0$ because of clutter. The right panel in Figure 10 compares the whitening processor's PCC simulations for the cases of known and unknown reflector locations. In this example, the uncertainty of reflector locations results in a 3–5 dB SNCR penalty.

5. CONCLUSION

This paper describes methods for assessing the target-classification performance of a SAR-based ATR for two specific target-constellation conditions: targets consisting of a known constellation of reflector components at known absolute locations and targets consisting of a constellation of known reflector components located at random positions within some limited, prescribed uncertainty regions. A lower bound on the PCC is obtained from the performance of a recognition processor that makes component-wise decisions on reflector types, and an upper bound on the PCC is obtained by assuming that the returns from the target components have known relative phases. Computer simulations showed that the lower bound is very close to the exact result for the known-reflector-position case. On the whole, for the examples we considered the optimum whitening-filter processor has approximately 6 dB gain in terms of SNCR compared to the conventional full-resolution processor. Some of the performance gain might be realized with an adaptive-resolution processor.

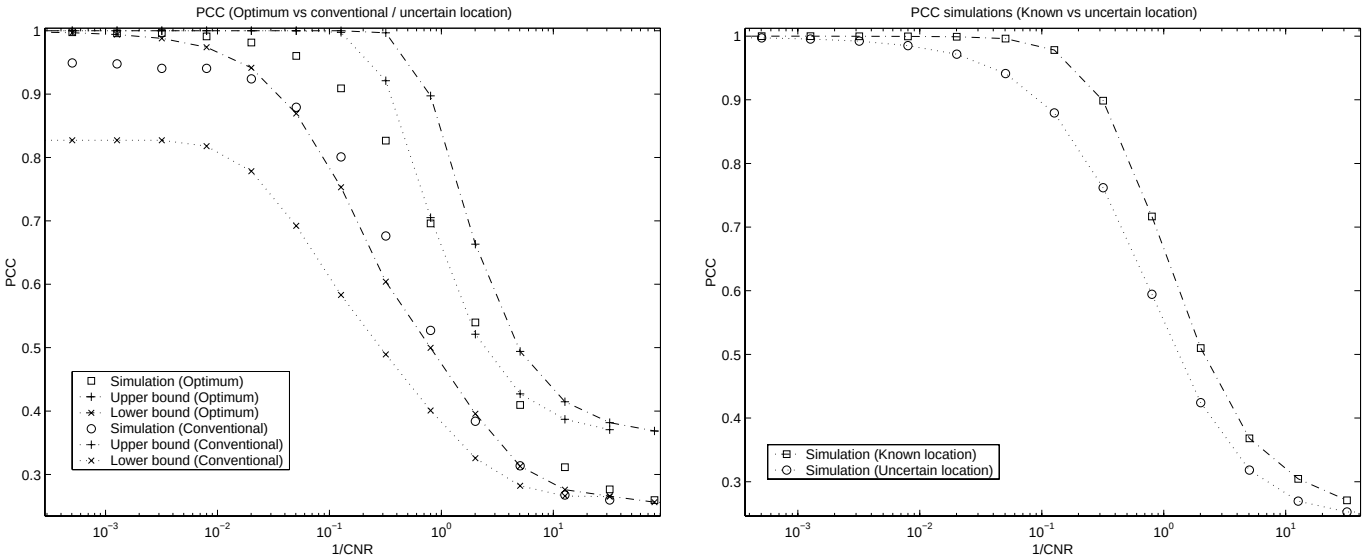

Figure 10. PCC upper and lower bounds for the target constellation specified in Table 3 and with a location uncertainty area of 30 cm by 30 cm for each reflector

REFERENCES

1. D. E. Dudgeon and R. T. Lacoss, "An overview of automatic target recognition," *Lincoln Laboratory Journal* **6**, pp. 3–10, 1993.
2. G. Leung and J. H. Shapiro, "Toward a fundamental understanding of multiresolution SAR signatures," *Proceedings of the SPIE* **3070**, pp. 100–109, 1997.
3. C.-P. Yeang and J. H. Shapiro, "Target detection theory for stripmap SAR using physics-based multiresolution signatures," *Proceedings of the SPIE* **3370**, pp. 646–660, 1998.
4. C.-P. Yeang and J. H. Shapiro, "Target identification for stripmap- and spotlight-mode SARs using physics-based signatures," *Proceedings of the SPIE* **3721**, pp. 748–762, 1999.
5. G. E. Séguin, "A lower bound on the error probability for signals in white Gaussian noise," *IEEE Transactions on Information Theory* **44**, pp. 3168–3175, Nov 1998.
6. J. C. Henry, "The Lincoln Laboratory 35 GHz airborne SAR imaging radar system," *Proceedings of IEEE National Telesystems Conference* , pp. 353–358, 1991.